AIP Publishing

This manuscript was accepted by Appl. Phys. Lett. Click here to see the version of record.

Unidirectional Distributed Acoustic Reflection Transducers for Quantum Applications

É. Dumur,[1,2] K. J. Satzinger,[3,1,a)] G. A. Peairs,[3,1] Ming-Han Chou,[1,4] A. Bienfait,[1] H.-S. Chang,[1] C. R. Conner,[1] J. Grebel,[1] R. G. Povey,[1,4] Y. P. Zhong,[1] and A. N. Cleland[1,2,b)]

[1)] *Institute for Molecular Engineering, University of Chicago, Chicago IL 60637, USA*

[2)] *Institute for Molecular Engineering and Materials Science Division, Argonne National Laboratory, Argonne, IL 60439, USA*

[3)] *Department of Physics, University of California, Santa Barbara CA 93106, USA*

[4)] *Department of Physics, University of Chicago, Chicago IL 60637, USA*

Recent significant advances in coupling superconducting qubits to acoustic wave resonators has led to demonstrations of quantum control of surface and bulk acoustic resonant modes as well Wigner tomography of quantum states in these modes. These advances were achieved through the efficient coupling afforded by piezoelectric materials combined with GHz-frequency acoustic Fabry-Perot cavities. Quantum control of *itinerant* surface acoustic waves appears in reach, but is challenging due to the limitations of conventional transducers in the appropriate GHz-frequency band. In particular, GHz-frequency unidirectional transducers would provide an important addition to the desired quantum toolbox, promising unit efficiency with directional control over the surface acoustic wave emission pattern. Here we report the design, fabrication and experimental characterization of unidirectional distributed acoustic reflection transducers (DARTs) demonstrating a high transduction frequency of 4.8 GHz with a peak directivity larger than 25 dB and a directivity greater than 15 dB over a bandwidth of 17 MHz. A numerical model reproduces the main features of the transducer response quite well, with ten adjustable parameters (most of which are constrained by geometric and physical considerations). This represents a significant step towards quantum control of itinerant quantum acoustic waves.

ACCEPTED MANUSCRIPT

Surface acoustic waves are typically launched and received using interdigital transducers (IDTs), comprising parallel metal fingers evenly spaced on a piezoelectric substrate. The center frequency f_0 of the transducer corresponds to an acoustic wavelength λ_0 twice the lateral spacing p of the fingers, where the frequency and wavelength are related by $f_0 = v_e/\lambda_0$, where v_e is the effective surface velocity in the transducer structure. The transducer bandwidth scales inversely with the number N of transducer fingers[1]. These structures have been used for many years, providing a convenient, inexpensive, and highly flexible approach to integrating acoustic-wave resonators, delay lines and pulse shaping with semiconductor electronics. Recently, in a pioneering experiment[2], a superconducting qubit was coupled to surface acoustic waves (SAWs) using an IDT transducer, the circuit fabricated on a GaAs substrate with a center frequency of about 5 GHz. This experiment allowed the low-temperature observation of quantum effects mediated by SAW phonons, the quanta of mechanical vibrations, coupled to the qubit through the IDT structure. More recently, other advances in the quantum control of surface acoustics have been demonstrated[3–5], showing promise for the expansion of this area of quantum physics.

A general challenge associated with uniform IDTs is that a voltage tone applied to the IDT will result in symmetric, oppositely-directed SAWs being emitted from the two ends of the IDT, effectively acting as a three-port device, with one electrical and two acoustic channels. This is appropriate for resonant structures where the IDT is placed between a pair of Fabry-Perot-like acoustic mirrors[1,3–5], but leading to the loss of half the acoustic power when used for example in a delay-line geometry. For this reason, unidirectional transducers (UDTs) are typically used to preserve acoustic power, using a more complex finger geometry or multiple phase-controlled electrical signals to emit and receive waves in a single direction. In the limit of very high directivity, a UDT can be viewed as a two-port device with one electrical and one acoustic channel, transducing signals between the two modes without loss. Future quantum applications would greatly benefit from high-directivity UDTs working in the GHz frequency band.

SAW directionality in UDTs is usually achieved using variants of IDT finger geometries designed to give constructive interference for waves emitted in one direction, and destructive interference for those in the opposite direction. Multi-phase UDTs offer very high directivity[1] but have complex finger geometries and require two or more phased voltage sources, making both fabrication and operation challenging. By contrast, single-phase UDTs (SPUDTs) achieve reasonable directivity using only a single voltage source, by using an asymmetric finger geometry. Since their introduction in 1976[6], these transducers have been implemented in a number of different formats[7–15].

One interesting approach to SPUDTs, termed a dis-

[a)] Present address: Google, Santa Barbara, California 93117, USA
[b)] Corresponding author: anc@uchicago.edu

This manuscript was accepted by Appl. Phys. Lett. Click here to see the version of record.

tributed acoustic reflection transducer (DART)[1,9], is a design that achieves high directivity by shifting the center of transduction from the center of reflection by a distance $3\lambda_0/8$, yielding the desired oppositely-directed constructive and destructive interference. Traditionally these have only been used at lower frequencies, below 100 MHz, with isolated examples up to 500 MHz[12,14]. The great simplicity of fabrication and operation makes these devices appealing for quantum operations if they can be made to work at higher (GHz) frequencies, compatible with superconducting qubits. Reaching such frequencies requires a careful iterative determination of the transducer parameters, and solving some challenges in the fabrication of long and narrow fingers on somewhat uncooperative substrates. Here we demonstrate a DART design that works well at frequencies approaching 5 GHz, an order of magnitude increase from prior work.

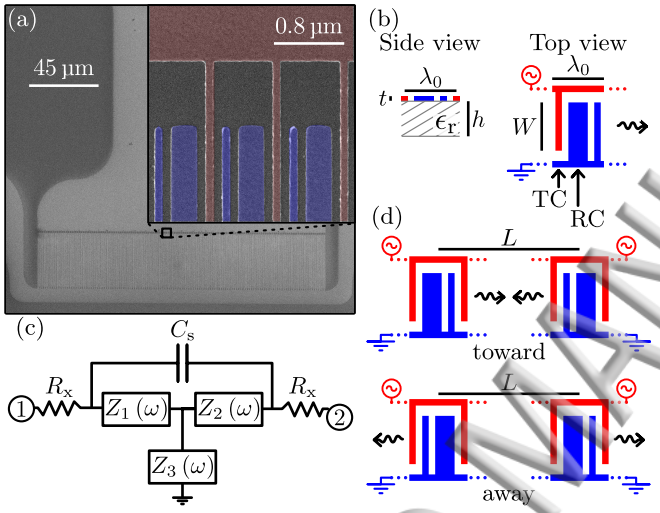

FIG. 1. (a) Scanning electron micrographs of a DART, with inset showing the drive and ground electrodes, driven electrodes in red and grounded electrodes in blue. (b) Side and top view of a unitary DART cell (thickness t exaggerated). (c) Complete equivalent electrical circuit of a delay line with $Z_{1,2,3}(\omega)$ the frequency-dependent impedances as predicted by the RAM and COM theories (see main text), with embedding resistance R_x and capacitance C_s. (d) Schematic "toward" and "away" DART configurations.

We designed and measured various DART designs, measuring single transducers as well as paired transducers in a delay line configuration, to fully characterize the transducer properties. The standard design is shown in Fig. 1, comprising driven transducer fingers of width $\lambda_0/8$ spaced by λ_0, interspersed with a $3\lambda_0/8$- and a $\lambda_0/8$-wide pair of grounded fingers with $\lambda_0/8$ inter-finger spacing. It has been shown that smaller thickness fingers leads to less surface-to-bulk mode conversion[16] but also decreases the reflectivity[1], so a compromise is made on the metal transducer thickness. We pattern the UDTs as a single layer of aluminum of thickness $t \approx 28$ nm on top of a single-side polished LiNbO3-128YX wafer of thickness $h = 500$ µm and room-temperature permittivity $\epsilon_r = 56$. The aluminum film is lift-off patterned by electron-beam lithography, using a polymethylmethacrylate (PMMA) bilayer composed of a 100 nm thick 495 kD weight bottom layer and a 100 nm thick 950 kD weight top layer. A 10 nm thick layer of Au is thermally evaporated on the top PMMA layer to reduce charging effects. The DART geometry is kept constant along the entire transducer length, with center wavelength $\lambda_0 = 800$ nm, corresponding to a center frequency f_0 just below 5 GHz.

We designed arrays of transducers in delay-line configurations, each delay line containing a pair of DARTs, typically with a center-to-center distance $L = 400\,\mu\text{m} = 500\,\lambda_0$. In a typical test set of devices, we would pattern an array of samples with different transducers apertures $W = \{18, 21, 24\}$ µm and different numbers of repeat cells, $N = \{125, 130, 135\}$. Each set of transducers was fabricated in two delay-line configurations, one where the DARTs are designed to emit towards one another, and one in the opposite configuration, where they emit away from one another (Fig. 1(d)).

Measurements were made at room temperature with a vector network analyzer, using a calibrated microwave probe station. We measured both reflection $S_{11} \cong S_{22}$ and transmission $S_{21} \cong S_{12}$ between pairs of DARTs in a delay-line configuration, with typical room-temperature results shown in Fig. 2.

For the transmission measurements, we show both the "towards" and "away" configurations, allowing us to extract the transducer directivity, a measure of the directionality of the acoustic power emission.

Over a broad frequency range, the reflection S_{11} and transmission S_{21} show the expected behavior, which away from the design frequency f_0 is dominated in reflection by the interdigital capacitance of the transducers, and in transmission by the stray electrical coupling between the two transducers. For our design, the stray electrical coupling is less than -60 dB for most of the frequency range of the measurement from 10 MHz to 7 GHz. Near the design center frequency $f_0 = 4.8$ GHz, we see the expected detailed frequency response for both reflection and transmission. There is a pronounced difference in the transmission for the "towards" and "away" transducer configurations, as expected for these directional transducers.

The detailed response near resonance is accurately captured by a model that takes into account the properties of the $LiNbO_3$ wafer, the aluminum electrodes and the microwave measurement circuitry. A schematic of the equivalent circuit model is shown in Fig. 1. (c), including the transducers and the delay line equivalent impedances Z_{1-3}, and an approximate embedding circuit comprising a series resistance $R_x \approx 15\,\Omega$ associated with the electrodes, and a stray capacitive coupling $C_s \approx 0.9$ pF between the two DARTs. These two parameters provide the broad frequency response for both S_{11} and S_{21}, away from the design frequency f_0.

To model the details of the DART response, we use the quasi-static approximation[1] to calculate the surface

ACCEPTED MANUSCRIPT

This manuscript was accepted by Appl. Phys. Lett. Click here to see the version of record.

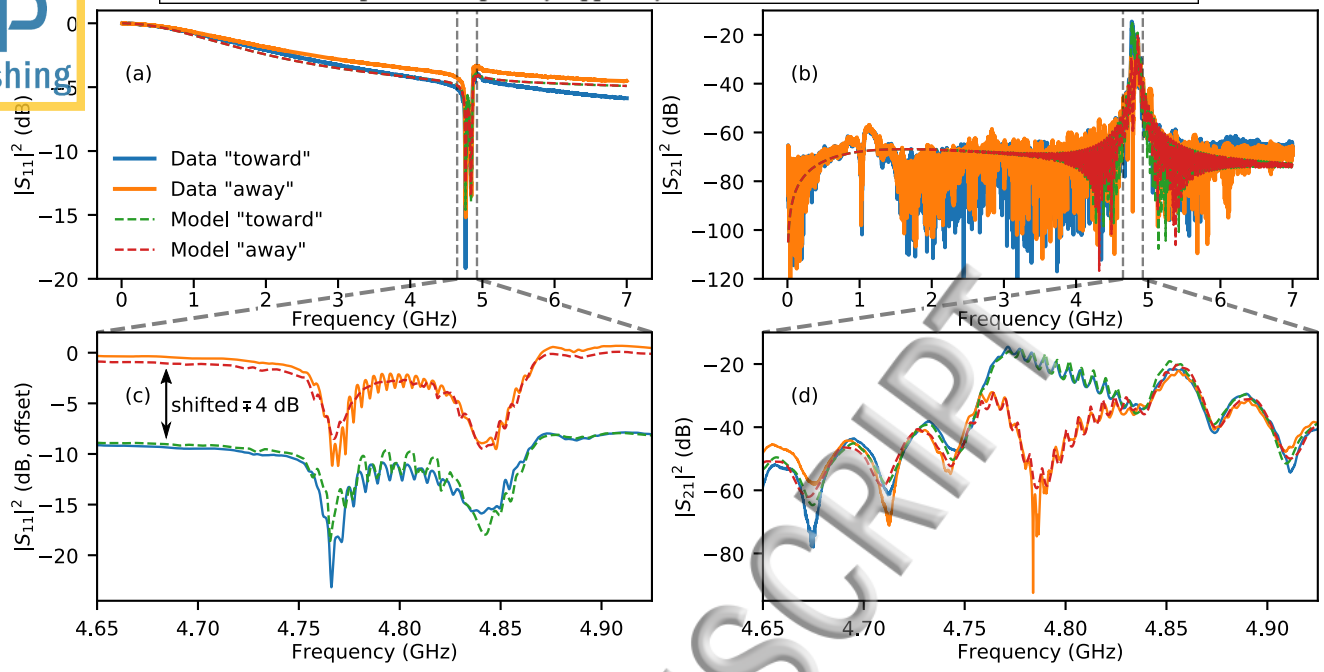

FIG. 2. DART paired response (S_{11} and S_{21}) as a function of frequency, for the "towards" and "away" configurations, using solid lines, compared with numerical modeling using dashed lines. The two configurations have similar response over a broad frequency range (a-b) except near the center design frequency (c-d), where the DART directivity is manifested.

wave power as well as the electrical charge density and the DART capacitance. The wide $3\lambda_0/8$ grounded electrode of the DART is modeled as two electrodes, spaced by $\lambda_0/8$, an approximation that has been shown to be valid at lower frequencies[17]. The effective wave velocity v_e is estimated using a first-order expansion developed for single finger pair IDTs and used here as an approximation[1], where $v_e = v_f + \Delta v_e + \Delta v_m$, with v_f being the free-surface SAW velocity, Δv_e the velocity change due to electrical loading, and Δv_m the velocity change due to mechanical loading. The reflection, transduction, conductance and susceptance of the DARTs are modeled through the coupling-of-modes (COM) theory[1], which models the DART cells as equally-spaced point contacts that couple the SAW modes traveling in one direction to the modes traveling in the opposite direction, through the electrical current flowing in the microwave circuit. The COM theory has two critical parameters, the transduction and reflection of each DART cell. Following Ref. 1, we use the reflective array method (RAM) to relate the transduction to the surface wave power and electrostatic charge density; while the RAM theory was not developed for DART-style transducers, elsewhere it has been shown that this is a reliable modeling approach[18]. The reflection is kept as a fitting parameter, which we restrict to be imaginary-valued, equivalent to assuming that transmission loss in the substrate dominates over transducer-associated losses.

In the reflection signal near resonance, the response consists of two local minima near 4.77 GHz and 4.84 GHz, separated by a broader local maximum. This is a characteristic of UDT-style transducers[1]. The reflection minima are at the frequencies where transmission is maximal, and the small ∼6 MHz ripples between the minima are due to interference between single and triple transit signals between the two transducers.

In the transmission signal near resonance, the overall signal level increases by more than 40 dB over the background stray coupling, with fine ripples due to interference effects within each transducer. The most striking feature is the strong difference in transmission between the "toward" and "away" DART configurations, due to the strong directivity of the transducer design. This directivity-dominated feature is more than 30 dB over a span of about 15 MHz centered at 4.785 GHz. The asymmetry of the response about the operating frequency is thought to be due to SAW velocity dispersion and the frequency-dependent reflectivity[1]. There is a slight frequency difference in the maximum transmission for the "toward" configuration compared to the minimum in the "away" configuration, attributed to the impedance mismatching of the transducers to the system 50 Ω impedance.

Fitting the detailed model to the data, we can extract the free velocity $v_f = 3865\,\mathrm{m\,s^{-1}}$, 3 % slower than in the literature[1], and the piezoelectric coupling $\Delta v/v = 1.9\,\%$, where for a similar two-finger SPUDT design, but at a lower center frequency, a comparison value[14] is $\Delta v/v = 1.5\,\%$. The shape of the overall response gives the imaginary reflectivity $r_s = i\,0.04$, which is roughly 30 % higher than the RAM estimate for this geometry. We note that the positive sign for the reflectivity is expected for this

ACCEPTED MANUSCRIPT

This manuscript was accepted by Appl. Phys. Lett. Click here to see the version of record.

type of substrate, and is responsible for inverting the preferred emission direction for this DART design compared to other substrate choices[1]. The fit geometric DART capacitance of 1.43 pF is 22 % smaller than the RAM estimate. While this represents a sizeable discrepancy, this is consistent with other experiments we have completed with significantly different designs but at similar frequencies on similar substrates[5].

The rapid oscillations in the transmission signal near the operating frequency are due to interference of signals in the delay line, and give us a very precise way to measure the effective distance between the two transducers, which is 400.08 µm, 0.02 % longer than geometric center-to-center design distance. The position of the minimum dip in the "away" configuration is determined by the distance between the transduction (TC) and reflection (RC) centers, $3\lambda_0/8$ by design, and is used as a fit parameter in the RAM theory. The numerical comparison yields a RC-TC distance 4 % larger than the design value.

The DART directivity is defined[1] as the ratio of the relevant P-matrix couplings, $D = |P_{13}/P_{23}|$. As these are not experimentally accessible, we instead use the approximate expression

$$D \approx \sqrt{\left|\frac{S_{21,t}}{S_{21,a}}\right|}, \qquad (1)$$

the square root of the ratio of the transmission scattering parameters in the "towards" (t) and "away" (a) configurations. The directivity is shown in Fig. 3, where in (a) we show the directivity from the full frequency-dependent signal, and in (b) we show the directivity when the delay line response is filtered in the time domain to isolate the response from the first transit signal through the delay line, as shown in (c). We note that without filtering, the apparent peak directivity is as high as 37 dB, but by selecting only the signal associated with the first transit, we find a more accurate measure of the peak directivity of 23 dB. This device has a bandwidth of 15 MHz, defined as the frequency range over which the directivity exceeds 15 dB.

We have measured a number of different DART configurations and tabulated representative results in Table I, using the first-transit filtered data for each design. The highest directivity was measured to be $D \approx 27$ dB for an aperture $W = 18$ µm, with $N = 125$ cells. The largest bandwidth was ≅ 17 MHz. The directivity shows a weak dependence on DART aperture, with larger apertures giving slightly lower directivity and smaller bandwidth, with the change mostly due to an increase in the "away" transmission.

In conclusion, we have fabricated DARTs with a high center frequency of 4.8 GHz, demonstrating a directivity greater than 15 dB over a bandwidth of 17 MHz. While highly promising, more study should be devoted to understanding the performance as a function of the transducer electrode dimensions. Future work should study the dependence of the directivity and bandwidth on parameters such as the metal electrode thickness, as well as the electrode and inter-electrode width ratio, which here were kept close to unity. The bandwidth of the DART could be increased by using slanted fingers[19]. A weighted or resonant design[1,20] could also sharpen and flatten the DART transduction peak response. The performance demonstrated here is promising for experiments in the quantum limit.

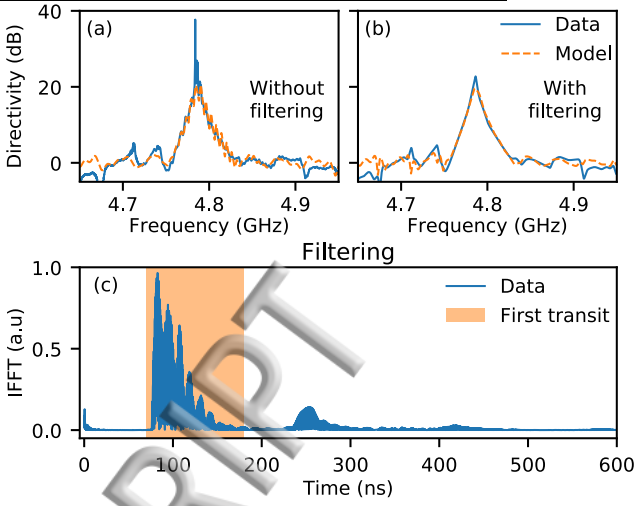

FIG. 3. DART directivity D, see Eq. (1), from data in Fig. 2. Solid and dashed lines represent the data and model, respectively. (a) Unfiltered data. (b) Data set filtered in time as per panel (c), representing the first transit peaking starting at ≅ 77 ns, and the third transit starting at ≅ 235 ns. Data are selected from the first transit, from 70 ns to 180 ns (colored band), and used to calculate the directivity in (b).

N	Aperture (µm)	D (dB)	BW (MHz)
125	18	26.89	16.75
	21	22.76	15.10
	24	20.38	15.95
130	18	25.89	16.00
	21	23.21	15.85
	24	19.36	15.20
135	18	23.16	16.90
	21	23.38	14.90
	24	20.04	16.35

TABLE I. Summary of different DART designs with their measured directivities and bandwidths. N is the number of cells, D the directivity and BW the bandwidth over which the directivity is greater than 15 dB.

SUPPLEMENTARY MATERIAL

See supplementary material for the derivation of the approximate directivity formula (Eq. 1) and a discussion of its validity.

ACCEPTED MANUSCRIPT

This manuscript was accepted by Appl. Phys. Lett. Click here to see the version of record.

ACKNOWLEDGMENTS

Devices and experiments were supported by the Air Force Office of Scientific Research and the Army Research Laboratory, and material for this work was supported by the Department of Energy (DOE). É. D. was supported by LDRD funds from Argonne National Laboratory, K.J.S. was supported by NSF GRFP (NSF DGE-1144085) and A.N.C. was supported by the DOE, Office of Basic Energy Sciences. This work was partially supported by the UChicago MRSEC (NSF DMR-1420709) and made use of the Pritzker Nanofabrication Facility, which receives support from SHyNE, a node of the National Science Foundations National Nanotechnology Coordinated Infrastructure (NSF NNCI-1542205).

[1]D. Morgan, Surface acoustic wave filters, 2nd ed. (Elsevier Ltd., 2007).
[2]M. V. Gustafsson, T. Aref, A. F. Kockum, M. K. Ekström, G. Johansson, and P. Delsing, Science **346**, 207 (2014).
[3]R. Manenti, A. F. Kockum, A. Patterson, T. Behrle, J. Rahamim, G. Tancredi, F. Nori, and P. J. Leek, Nature Communications **8**, 975 (2017).
[4]B. A. Moores, L. R. Sletten, J. J. Viennot, and K. W. Lehnert, Phys. Rev. Lett. **120**, 227701 (2018).
[5]K. J. Satzinger, Y. P. Zhong, H.-S. Chang, G. A. Peairs, A. Bienfait, M.-H. Chou, A. Y. Cleland, C. R. Conner, . Dumur, J. Grebel, I. Gutierrez, B. H. November, R. G. Povey, S. J. Whiteley, D. D. Awschalom, D. I. Schuster, and A. N. Cleland, Nature **563**, 661 (2018).
[6]K. Hanma and B. J. Hunsinger, in 1976 Ultrasonics Symposium (1976) pp. 328–331.
[7]C. S. Hartmann, P. V. Wright, R. J. Kansy, and E. M. Garber, in 1982 Ultrasonics Symposium (1982) pp. 40–45.
[8]M. Lewis, in 1983 Ultrasonics Symposium (1983) pp. 104–108.
[9]T. Kodama, H. Kawabata, Y. Yasuhara, and H. Sato, in IEEE 1986 Ultrasonics Symposium (1986) pp. 59–64.
[10]J. M. Hode, M. Doisy, and P. Dufilie, in IEEE Symposium on Ultrasonics, Vol. 1 (1990) pp. 429–434.
[11]K. Yamanouchi, C. H. S. Lee, K. Yamamoto, T. Meguro, and H. Odagawa, in IEEE 1992 Ultrasonics Symposium Proceedings, Vol. 1 (1992) pp. 139–142.
[12]E. M. Garber, D. S. Yip, and D. K. Henderson, Proceedings of IEEE Ultrasonics Symposium **1**, 7 (1994).
[13]S. Lehtonen, V. P. Plessky, C. S. Hartmann, and M. M. Salomaa, IEEE Transactions on Ultrasonics, Ferroelectrics, and Frequency Control **50**, 1404 (2003).
[14]G. Martin, S. V. Biryukov, H. Schmidt, B. Steiner, and B. Wall, IEEE Transactions on Ultrasonics, Ferroelectrics, and Frequency Control **58**, 658 (2011).
[15]K. Yamanouchi, Z. H. Chen, and T. Meguro, in IEEE 1986 Ultrasonics Symposium (1986) pp. 81–84.
[16]Y. Ebata, in IEEE 1988 Ultrasonics Symposium Proceedings. (1988) pp. 91–96 vol.1.
[17]P. Dufilie and P. Ventura, in IEEE Ultrasonics Symposium, Vol. 1 (1995) pp. 13–16.
[18]D. P. Morgan, IEEE Transactions on Ultrasonics, Ferroelectrics, and Frequency Control **45**, 152 (1998).
[19]H. Yatsuda, Y. Takeuchi, and S. Yoshikawa, in IEEE Symposium on Ultrasonics, Vol. 1 (1990) pp. 61–66.
[20]P. Ventura, M. Solal, P. Dufilie, J. M. Hode, and F. Roux, in 1994 Proceedings of IEEE Ultrasonics Symposium, Vol. 1 (1994) pp. 1–6 vol.1.

ACCEPTED MANUSCRIPT

(a)

45 µm

0.8 µm

(b)

Side view

λ_0

t

ϵ_r

h

Top view

λ_0

W

TC

RC

(c)

C_s

R_x

R_x

1

2

$Z_1\,(\omega)$

$Z_2\,(\omega)$

$Z_3\,(\omega)$

(d)

L

toward

L

away

ACCEPTED MANUSCRIPT

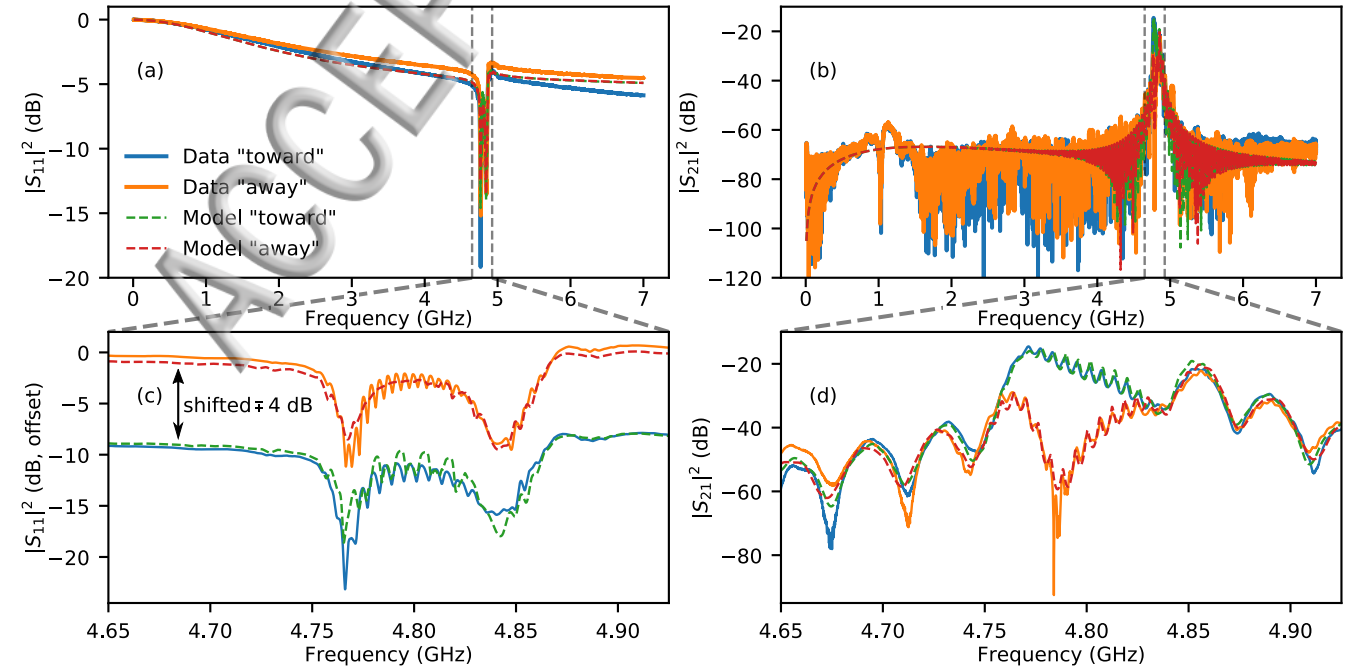
(a)
(b)
(c)
(d)
Data "toward"
Data "away"
Model "toward"
Model "away"
shifted ∓ 4 dB
$|S_{11}|^2$ (dB)
$|S_{21}|^2$ (dB)
$|S_{11}|^2$ (dB, offset)
Frequency (GHz)

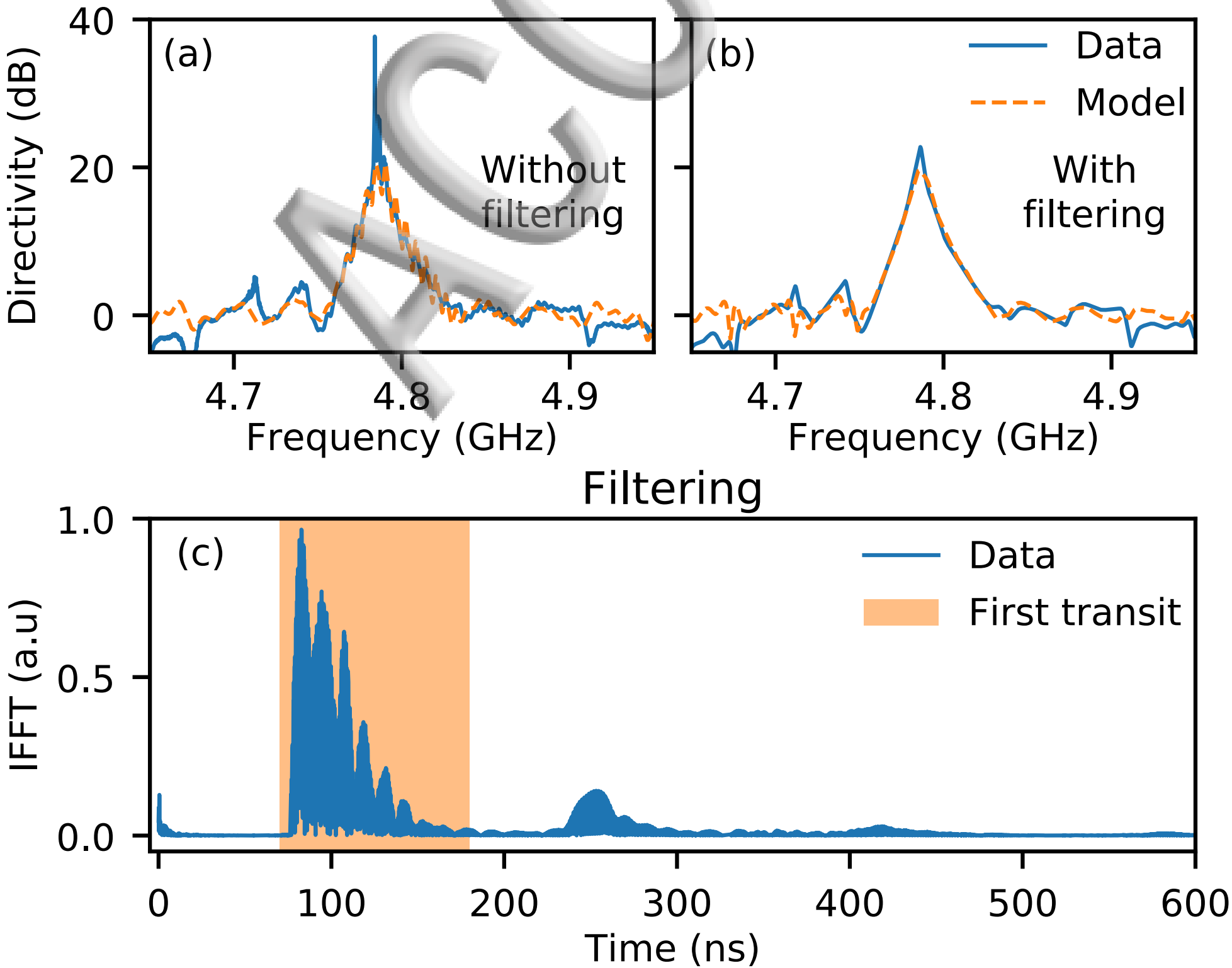
(a)
(b)
Data
Model
Without filtering
With filtering
Directivity (dB)
40
20
0
4.7
4.8
4.9
Frequency (GHz)
Filtering
(c)
Data
First transit
IFFT (a.u)
1.0
0.5
0.0
0
100
200
300
400
500
600
Time (ns)